LATVIAN JOURNAL OF PHYSICS
AND TECHNICAL SCIENCES
2025, N 6

DOI: 10.2478/lpts-2025-0041

INVESTIGATION OF Fe-Ni CATALYST DRYING INFLUENCE ON METHANE PYROLYSIS FOR TURQUOISE HYDROGEN PRODUCTION

A. Knoks[1*], L. Grinberga[1], R. K. Sika[1], V. Vitola[1],
S. Varnagiris[2], M. Urbonavicius[2], J. Kleperis[1†]

[1]Institute of Solid State Physics University of Latvia,
8 Kengaraga Str., Riga, LV-1063, LATVIA
[2]Center for Hydrogen Energy Technologies,
Lithuanian Energy Institute,
3 Breslaujos, Kaunas, 44403, LITHUANIA
*e-mail: ainars.knoks@cfi.lu.lv

Methane pyrolysis is a promising method for turquoise hydrogen production with reduced CO_2 emissions. This study investigates how drying of catalyst before pyrolysis influences catalyst surface and its relation to hydrogen production. The Fe–Ni catalyst system was prepared by magnetron sputtering onto γ-Al_2O_3 support. Structure and surface chemistry were analysed using FTIR, Raman spectroscopy, XPS, SEM, and XRD. Pre-treatment was found to remove hydroxyl and organic residues, alter Fe/Ni oxidation states, and influence carbon morphology after pyrolysis. Pyrolysis produced mainly nanostructured carbon (CNT and graphene-like) materials, while vacuum drying improved metal dispersion and reduced surface oxygen. The results were compared to pyrolysis outcomes at higher temperatures, showing that optimized catalyst pre-treatment enhanced hydrogen yield and carbon quality. Results supported not only the development of efficient catalysts for turquoise hydrogen production but also procedure importance.

Keywords: *Fe–Ni catalyst, methane pyrolysis, nanocarbon formation, pre-treatment, turquoise hydrogen, γ-Al_2O_3 support.*

1. INTRODUCTION

The transition to a low-carbon economy places hydrogen energy at the core of future energy systems. The European Union has outlined hydrogen as a cornerstone of its Hydrogen Strategy for a Climate-Neutral Europe, aiming to scale production and consumption across industrial sectors [1]–[3]. However, the cost and infrastructure challenges associated with renewable-based "green" hydrogen production via electrolysis remain substantial. Steam methane reforming (SMR), currently the dominant industrial process, emits large amounts of CO_2. Although carbon capture and storage (CCS) can mitigate these emissions, it adds considerable cost and operational complexity.

Methane pyrolysis has recently emerged as a promising alternative for turquoise hydrogen production, generating hydrogen and solid carbon without CO_2 emissions [4]–[6]. The process can operate with existing natural gas infrastructure while providing an additional revenue stream from valuable carbon nanomaterials. The main obstacle to industrial deployment is the lack of stable and efficient catalysts that can sustain high methane conversion while resisting deactivation by carbon deposition.

Bimetallic Fe–Ni catalysts supported on γ-Al_2O_3 have demonstrated strong activity in methane decomposition due to the synergistic interaction between the two metals. Nickel provides efficient methane dissociation, while iron enhances carbon diffusion and delays deactivation [7]–[9]. Catalyst pre-treatment – through drying, oxidation, or reduction – has a decisive influence on the metal oxidation state, particle dispersion, and overall activity [11]–[13]. Previous studies have shown that appropriate pre-treatment can promote the formation of active metallic sites and improve carbon morphology during methane cracking.

To simplify the pyrolysis process, robust catalysts should be used. Moreover, omission of classic reduction or pre-treatment can decrease overall operational complexity and costs. To that extent, the present study compares a sample drying effect on surface chemistry, oxidation state, and morphology of Fe–Ni catalysts prior to methane pyrolysis at 700 °C. Characterisation was performed using Fourier-transform infrared spectroscopy (FTIR), Raman spectroscopy, X-ray photoelectron spectroscopy (XPS), X-ray diffraction (XRD), and scanning electron microscopy (SEM). The results provide insight into how surface conditioning influences catalyst activation and carbon nanostructure formation, contributing to the optimisation of Fe–Ni catalysts for turquoise hydrogen production [14], [15].

2. EXPERIMENTAL

2.1. Catalyst Preparation

Fe catalysts embedded with Ni nanoclusters were synthesised by physical vapor deposition (PVD) using a dual-magnetron PVD 75 system (Kurt J. Lesker Co.). High-purity Fe and Ni (99.99 %) targets were employed, while γ-Al_2O_3 powder (Testbourne, 99.99 %, 130 ± 20 m^2/g) served as the substrate. The deposition chamber

was evacuated to a base pressure of 5×10^{-7} mbar and subsequently filled with Ar gas to a working pressure of 6×10^{-3} mbar. Fe deposition was carried out at 0.8 A and 380 V for 5 minutes. Ni nanoclusters were deposited at 0.3 A and approximately 360 V for 18 seconds to promote discrete cluster formation and prevent continuous film growth. To ensure uniform metal dispersion, a two-step deposition procedure was applied for both Fe and Ni, with intermediate manual mixing of the γ-Al_2O_3 powder between cycles.

2.2. Catalyst Pre-treatment

To assess the influence of adsorbed water and gas species on the catalyst properties, a series of samples was subjected to controlled thermal and vacuum treatments. The preparation steps included drying and pyrolysis procedures designed to remove physisorbed moisture and volatile components and examine the structural and surface changes induced by these processes. The detailed pre-treatment and post-treatment conditions for each sample are summarised in Table 1.

Table 1. Summary of Catalyst Pre-treatment and Post-treatment Conditions

Sample code	Description
7–1	As-prepared sample (no treatment)
7–2	7-1 dried at 120 °C for 1 h under constant vacuum (10^{-1} mbar).
7–3	Pyrolysed 7-1
7–4	7-3 dried at 120 °C for 1 h under constant vacuum (10^{-1} mbar).
7–5	Pyrolysed 7-2
7–6	7-5 + dried at 120 °C for 1 h under constant vacuum (10^{-1} mbar).

2.3. Methane Pyrolysis

Methane pyrolysis was performed in a custom-built fixed-bed quartz reactor (internal volume 2042 cm^3). The catalyst (1g) was placed in the reactor and purged with nitrogen (flow rate 1000 mL min^{-1}) to remove air. Methane (Linde, 99.9995 %) was introduced to a pressure of 0.5 bar, and the reactor was heated to a temperature of 700 °C at a rate of 5.83°C/min. The set temperature was held for 4 h, followed by natural cooling.

Gas-phase products were sampled into RESTEK stainless-steel bottles; gas sample was taken after cooling to room temperature and measured with mass spectrometer (RGA100 MS, Stanford Research Systems, Sunnyvale, CA, USA).

Gas calibration procedure for MS analysis was done via standardized reference gases with additional calibration on CO content via purchased flask (Linde, 99.96 %) to quantify mass spectra signal at various pressures for CO identification and quantification. Each sample was tested at least three times to diminish atmospheric contamination.

2.4. Characterisation

The structural and surface properties of the catalysts were characterised using various analytical techniques. Fourier transform infrared (FTIR) spectra were col-

lected using a Vertex 80v (Bruker) operating in the 10000 cm^{-1} to 10 cm^{-1} range at a resolution of 0.1 cm^{-1}. Raman spectra were obtained using a TriVista CRS Confocal Raman Microscope (Spectroscopy & Imaging GmbH) with a 532 nm excitation laser operating at a power of approximately 1.4 mW at the sample surface. X-ray diffraction (XRD) measurements were performed on a MiniFlex 600 (RIGAKU) diffractometer using Cu Kα radiation (λ = 1.5406 Å) at 40 kV and 15 mA, with a 2θ scan range of 20°–80° and a step size of 0.02°. X-ray photoelectron spectroscopy (XPS) was carried out using an ESCALAB Xi system (Thermo Fisher Scientific) equipped with Al Kα radiation (hν = 1486.6 eV), and all binding energies were referenced to the C 1s peak at 284.8 eV. Surface morphology was examined by scanning electron microscopy (SEM) using a Helios 5 UX instrument (Thermo Fisher Scientific) operated at an accelerating voltage of 5 kV and equipped with high-performance in-chamber electron and ion detectors.

2.5. Gas and Carbon Yield Analysis

The hydrogen yield and carbon mass gain were determined by correlating the detected gas composition with the catalyst mass before and after the reaction. The carbon yield was evaluated gravimetrically as the relative mass increase of the catalyst after pyrolysis, expressed in weight percent (wt%) with respect to the initial mass of catalyst, similarly as shown by Al-Fatesh et al. [20]. The hydrogen yield was calculated by normalizing converted hydrogen to 1 mol of CH_4. Calculations are taken from the measured hydrogen concentration in the gas phase, expressed in % of the total gas composition as ratio between final H_2 content and initial CH_4 content, considering other carbon containing molecules. Gas content data is obtained from mass spectrometric analysis.

3. RESULTS AND DISCUSSION

3.1. FTIR and Raman

To investigate the surface-adsorbed species, FTIR and Raman analyses were performed on the catalyst samples. As shown in Fig. 1a, the as-prepared samples exhibit strong O–H stretching bands, along with C–H, C–C, and pronounced C–O vibrations appearing slightly above 1500 cm^{-1} and 1000 cm^{-1}, respectively, which can be attributed to surface carbon species. After pyrolysis, the samples without prior drying or N_2 purging show the disappearance of the O–H and other associated functional groups. In contrast, partially retained O–H vibrations are observed in the dried samples, indicated by bands between 3500 and 3700 cm^{-1}. Broad Al–O modes are faintly visible in the 500–900 cm^{-1} region.

Raman spectroscopy is a powerful tool for identifying carbon atom vibrations: the D band corresponds to in-plane vibrations of disordered graphite, while the G band is associated with sp^2 carbon vibrations in a hexagonal lattice. The intensity ratio of D to G bands (I_D/I_G) provides insights into the number of carbon layers and the degree of crystallinity, as described by Ferrari and Robertson [13].

Obtained Raman spectra reveal no dis-

tinct carbon-related bands before pyrolysis, whereas pronounced D, G, and 2D modes appear after the reaction, indicating the formation of nanostructured carbon such as carbon nanotubes (CNTs) and graphene-like materials. Similar findings were reported by Sun et al. [16], where tubular CNTs were synthesized via methane pyrolysis. Comparing obtained Raman data with similar catalysts, such as in the study by Wang et al. [17], where the D band appeared at 1336 cm^{-1} and the G band at 1570 cm^{-1}, reveals that the I_D/I_G ratio varies with Fe content and catalyst support. Notably, the highest Fe loading (60 wt%) resulted in the most crystalline CNTs.

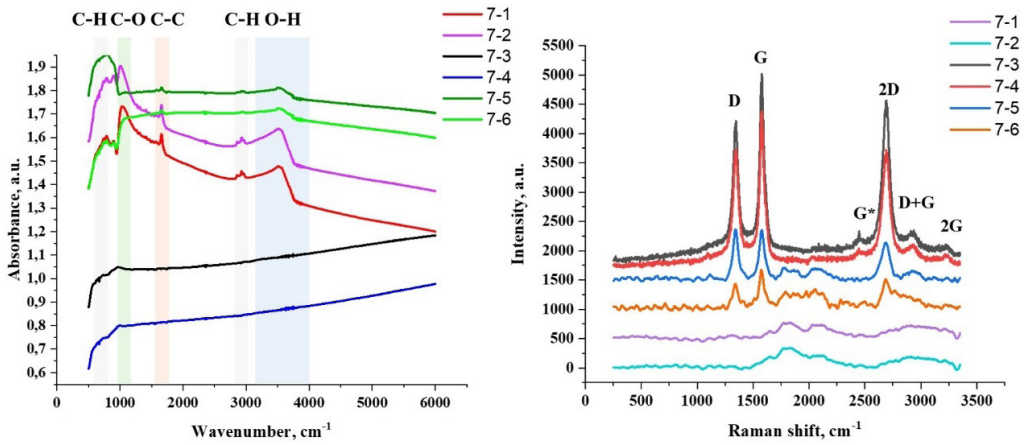

Fig. 1. FTIR and Raman spectra of samples. a) FTIR of the samples shows variations of surface b) Raman spectra of samples, different results of nanostructured carbon on the surface of catalysts.

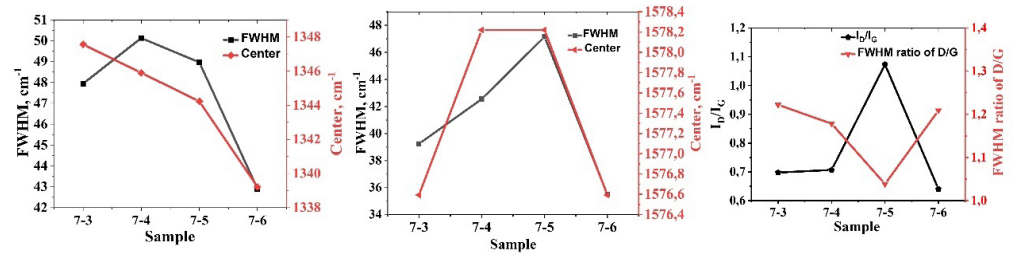

Fig. 2. Raman D and G mode position changes. a) D mode position and FWHM changes, b) G mode position and FWHM changes, c) defect evaluation via intensity I_D/I_G and FWHM ratio, changes in defect and structure composition are expected.

Comparing the visible spectral shifts when drying, as well as the increase in the I_D/I_G ratio, indicates a higher degree of disorder that partially arises from adsorbed species. As observed in the changes between samples 3 and 4, drying seemingly increases the disorder/defects, though the effect is relatively small. On the other hand, pyrolysis significantly enlarges the disorder due to the presence of adsorbed species, while subsequent drying reduces it again. These observations suggest that catalyst handling can influence the type of carbon structures that form during pyrolysis.

Similar results are reported in the literature for single and multi co-catalyst materials, such as Fe/Al_2O_3, clearly showing lower disorder/defect with this ratio coming to 0.7 [17]. Ni/Al_2O_3 exhibits a slightly higher ratio, just above 1; however, the $NiFe/Al_2O_3$ multi-catalyst system reduces the level of disorder, with the ratio slightly below 1 [18]. A more complex catalyst composition containing Fe, such as $Mo_{0.1}Fe_{0.05}Mg_{0.85}O_x$, shows a notably lower I_D/I_G ratio value of 0.44 [19]. These findings highlight the role of Fe in modulating the structure and form of carbon materials during growth.

3.2. XRD

Structural analysis using XRD reveals that the initial samples contain no detectable carbon, but exhibit the presence of Fe, as well as alumina. After pyrolysis, distinct carbon peaks appear along with the expected iron–carbon phases, while the intensity of iron oxide peaks decreases. As expected, drying prior to pyrolysis does not significantly affect the structure. However, drying after pyrolysis leads to a reduction in the C(004) peak, located just below 55° of 2 Theta.

This observation aligns with the XPS data shown in Fig. 3, where a decrease in carbon content is also evident. The correlation suggests that it can be assumed that certain amount of carbon is volatile and may be lost during post-processing. This has implications for the stability and usability of carbon material, particularly regarding its potential detachment from the sample surface.

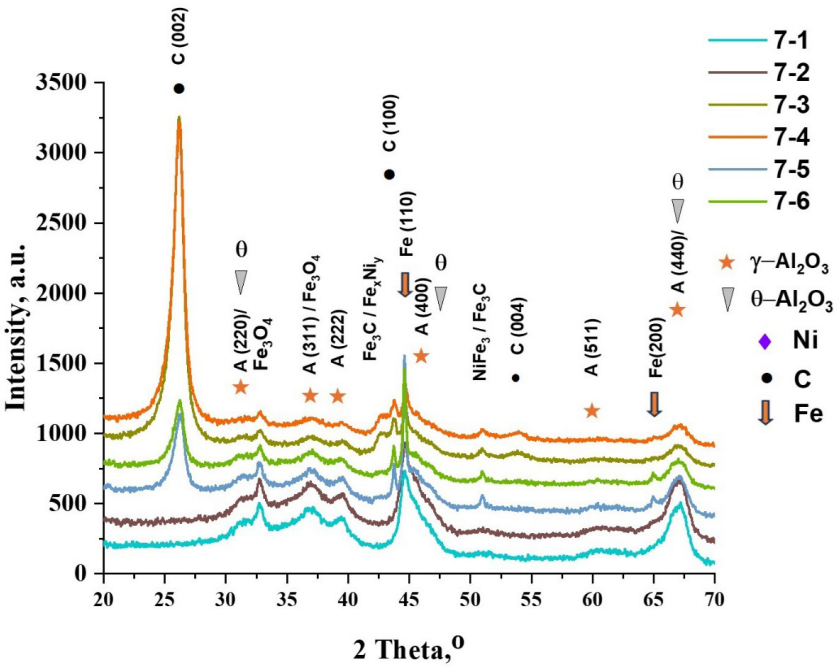

Fig. 3. XRD results of samples. Clear indication of carbon growth, as seen in samples after pyrolysis, via the appearance of the C(002) peak and the Fe_3C peak. At the same time, vacuum drying decreased the C(004) peak intensity.

3.3. XPS

To investigate the surface chemistry of the catalysts, XPS analysis was performed. The spectra revealed the presence of various elements, with notable variations in carbon and oxygen content (Fig. 4) depending on whether the samples underwent pyrolysis with or without prior drying. It is assumed that as-prepared samples contained adsorbed water, which could influence surface oxidation or promote the formation of CO and CO_2 during the reaction, thereby reducing efficiency of the hydrogen production.

XPS measurements were conducted to compare the surface composition of air-exposed, dried, and pyrolyzed samples. As shown in Fig. 4, mostly oxygen, carbon and aluminium were detected, where carbon content increased after pyrolysis, as expected. Notably, O is in two states, i.e., bound to support and adsorbed on the surface. In addition, small amounts of Fe and Ni were detected, along with trace quantities of nitrogen, fluorine, and cobalt, even in the dried samples.

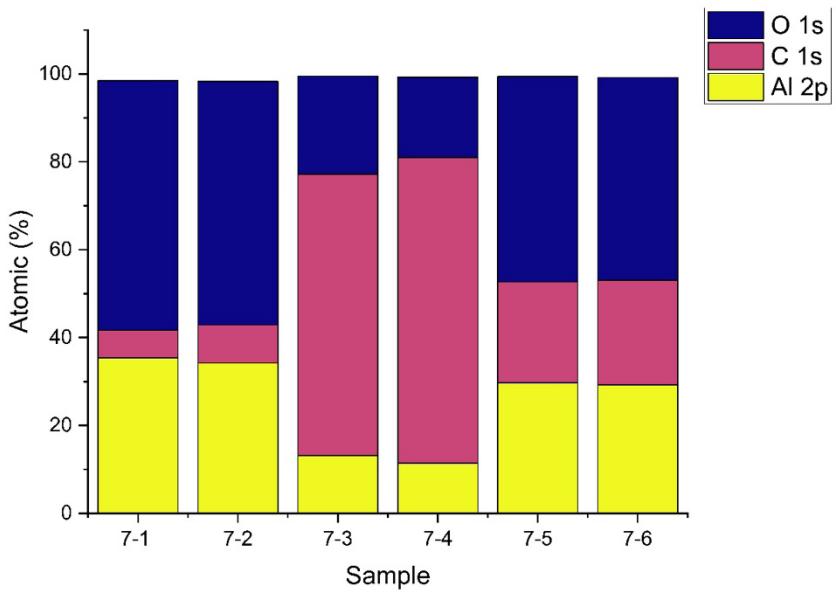

Fig. 4. Evaluation of drying influence on the surface, the main elements are as expected O, C, Al. Since the concentrations of trace elements were negligible compared to the major components, they are not presented for clarity.

To evaluate the oxygen species, present on the surface (Fig. 5), the relative oxygen content was quantified. A slight increase in lattice oxygen was observed after drying, suggesting the removal of adsorbed water and CO_2, although the overall change was minor (approximately 3 %). The pyrolyzed samples exhibited lower lattice oxygen content than the dried ones, while additional drying of sample 5 resulted in a small increase in lattice oxygen, indicating partial re-adsorption or residual oxygen incorporation.

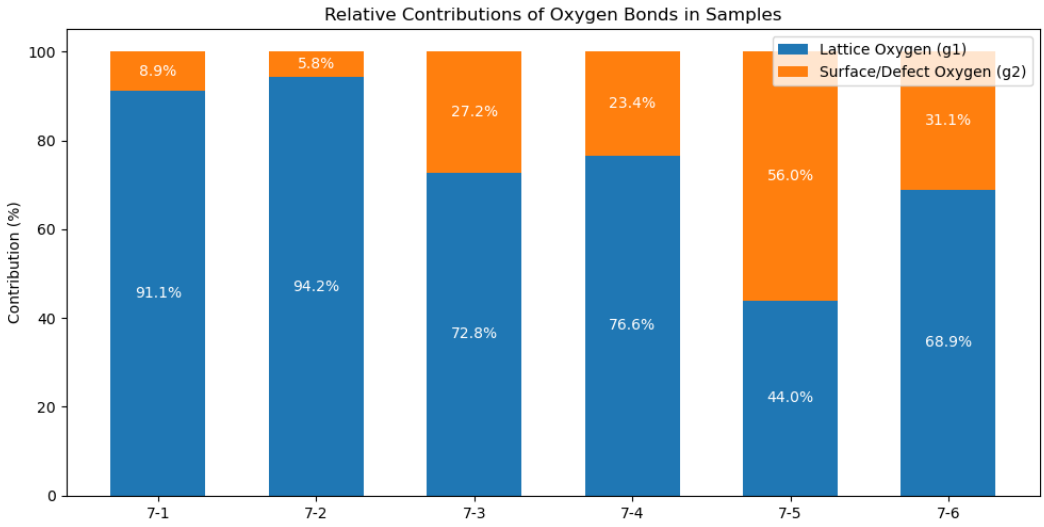

Fig. 5. Evaluation of drying influence on the surface oxygen content among samples.

3.4. Pyrolysis Reaction

The production of turquoise hydrogen is being explored as a promising transitional technology for cost-effective hydrogen generation. Catalysts play a key role in improving thermodynamic efficiency and reducing the reaction temperature, while also needing to remain robust and easy to handle. Wang et al. [17] reported catalyst deactivation within 60 minutes of methane pyrolysis, with the hydrogen yield decreasing from below 20 % at the start to slightly above 10 % after 60 minutes at 700 °C. In their previous study, the performance of Ni catalysts supported on γ-Al_2O_3 and modified with additives such as Mn, Cu, and Fe was investigated. The as-prepared Ni catalyst achieved a hydrogen yield of approximately 50 %, which increased to 5 3% with Fe addition and reached 78 % when Mn was introduced. However, all catalysts exhibited deactivation within 100 minutes, except for the Ni–Fe system, which maintained activity for about 200 minutes.

Zhang et al. [19] studied carbon materials produced by methane cracking at different temperatures and using various catalysts. They observed that most catalysts achieved hydrogen conversion rates below 50 %, except for CNO and CMB catalysts, which reached approximately 83 % and 77.6 %, respectively.

As reported in the literature, hydrogen yields vary widely depending on catalyst composition and reaction conditions. In this study (Fig. 6), a substantial increase in hydrogen content was observed after drying the samples. To assess the influence of this simple pre-treatment step, catalysts synthesized at 700, 800, and 900 °C were compared. SEM analysis was further employed to evaluate the resulting carbon morphologies. Interestingly, the dried sample at the lowest temperature (700 °C) demonstrated the highest overall efficiency, suggesting that appropriate catalyst pretreatment could enhance performance while potentially reducing operational costs.

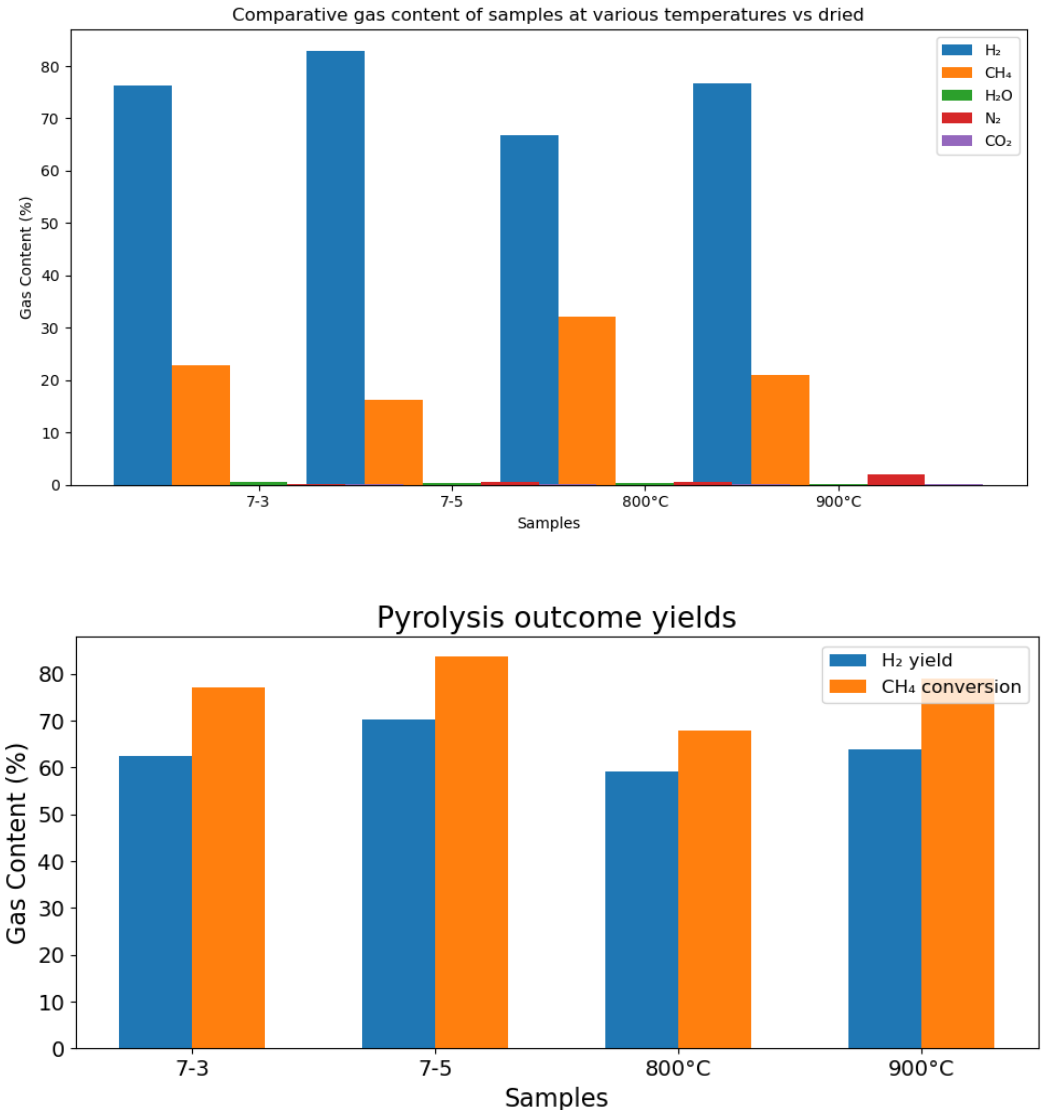

Fig. 6. Gas analysis results. Dried sample has higher hydrogen content compared to a pyrolyzed sample, even at higher temperature pyrolysis reactions.

Wang et al. [18] investigated various catalysts supported on γ-Al_2O_3 for methane pyrolysis. In the case of Ni/Al_2O_3 with different additives, thick carbon filaments were observed to grow on the catalyst surface, with the morphology slightly dependent on the type of co-catalyst. In a more detailed analysis using high-resolution transmission electron microscopy of carbon materials formed during CH_4 cracking, it was concluded that Fe and Ni catalysts promoted the formation of carbon nanotubes via a root-growth mechanism with closed tips. Interestingly, when comparing individual catalysts, Fe produced thinner-walled CNTs (2–5 graphene layers) with smaller inner diameters than those obtained using Ni.

3.5. SEM

In this study, highly fibrous carbon nanostructures (CNFs) were observed growing on the catalyst surface, consistent with the Raman spectroscopy results. The CNFs exhibited well-defined morphology with varying degrees of curvature, as shown in Fig. 7. When comparing catalyst mass gain, the dried samples showed a smaller increase compared to those pyrolyzed at higher temperatures (900 °C) or without drying. However, as indicated by both Raman and SEM analyses, the CNF/CNT structures formed under drying conditions appeared to possess higher structural quality and improved graphitic ordering.

7-1, as prepared

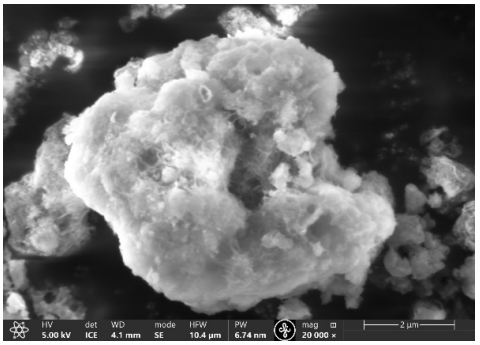

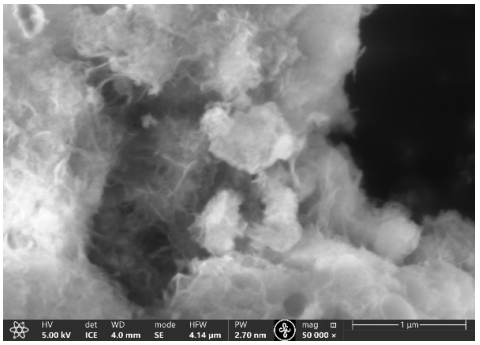

7-3, pyrolyzed 7-1 at 700 °C

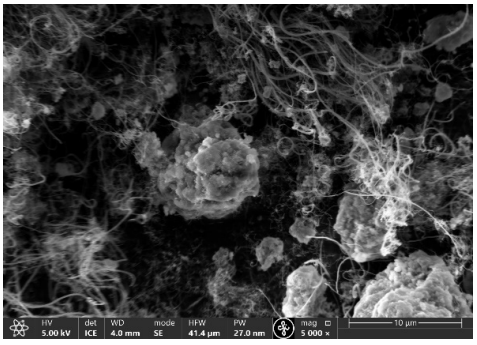

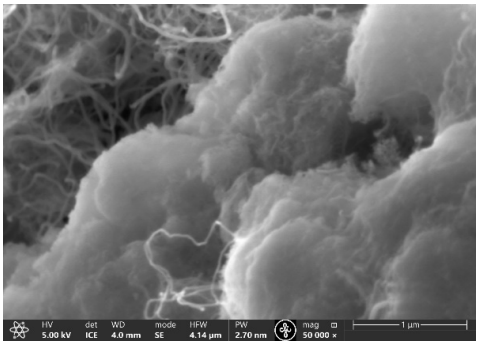

Pyrolyzed 7-1 at 800 °C

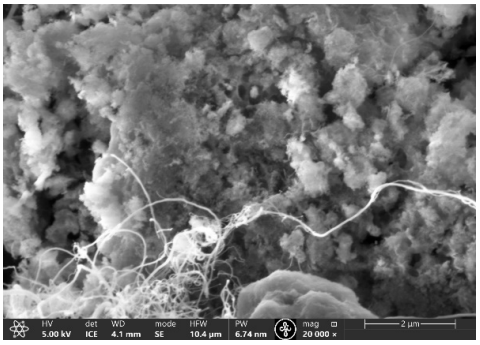

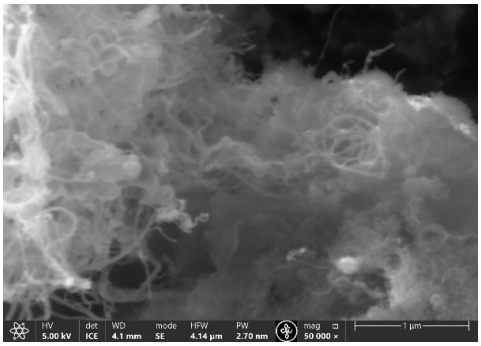

Pyrolyzed 7-1 at 900 °C

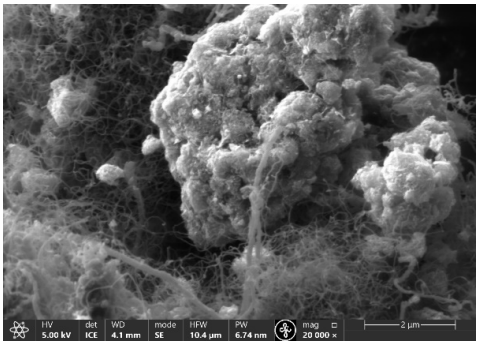

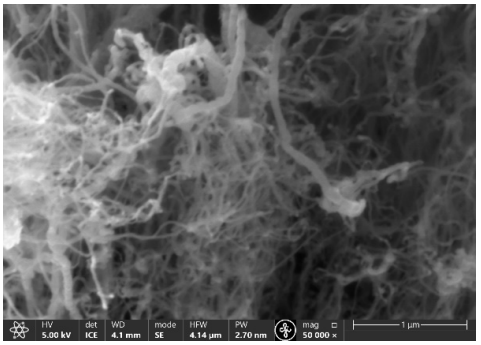

Pyrolyzed 7-2, dried at 120 °C for 1 h under constant vacuum (10^{-1} mbar).

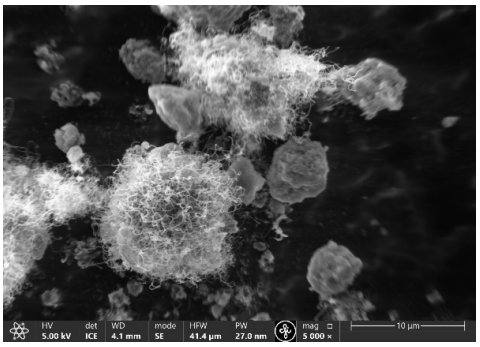

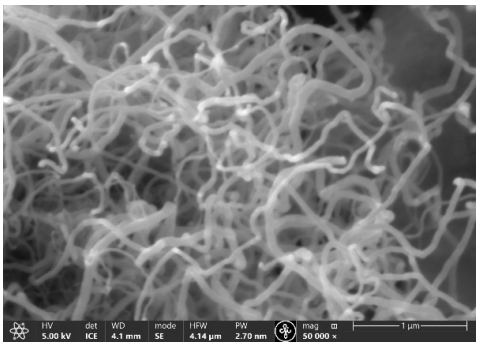

Fig. 7.

3.6. Carbon yield

The carbon deposition dependence on pyrolysis temperature is shown in Fig. 8. The results indicate that both temperature and sample pre-treatment influence the amount of deposited carbon. The Ni–Fe/Al_2O_3 catalyst demonstrated the highest carbon yield at 900 °C, reaching 180.6 %, while the sample pre-dried prior to pyrolysis at 700 °C achieved a carbon yield of 146.8 % with the highest hydrogen yield (70.2 %). These findings suggest mild drying enhances catalytic performance by improving surface activity and limiting oxygen-related inhibition.

A comparison of the obtained results with literature data is summarised in Table 2. The carbon yields reported in this study are notably higher than those observed for other catalyst systems, such as Fe–Co or Ni/Al_2O_3 formulations [18]–[20]. Moreover, the hydrogen yield and catalyst stability achieved with the Ni–Fe/Al_2O_3 catalysts are higher compared to the previously published results, confirming the effectiveness of this bimetallic system for methane pyrolysis.

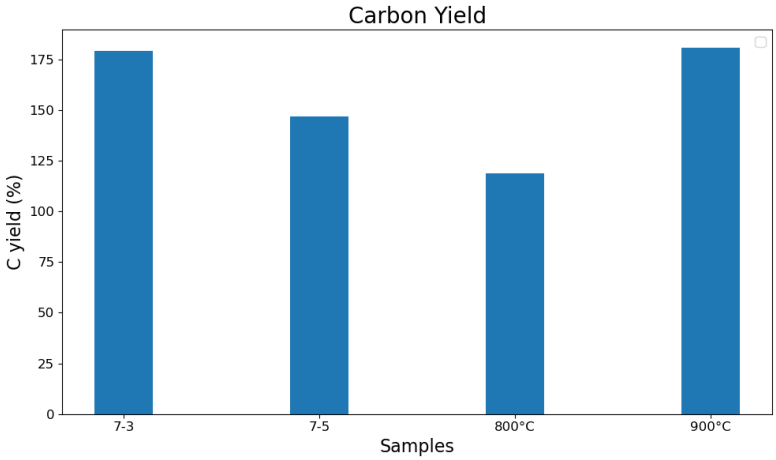

Fig. 8. Carbon deposition dependence on the sample processing/pyrolysis temperature.

Table 2. Summary of Carbon and Hydrogen Yields for Different Catalysts for Methane Pyrolysis

Catalyst	Temp	C yield, %	Peak H_2 yield, %	Time, h	Source
5 wt% Fe-60 wt% Ni/Al_2O_3		356,62	50	1/6	[18]
60 wt% Ni/Al_2O_3		98.41	53	1/6	[18]
$Mo_{0.1}Fe_{0.05}Mg_{0.85}O_x$	800	175	40	15	[19]
Ni-Fe/Al_2O_3	700	179.1	62.5	4	This study
Ni-Fe/Al_2O_3	800	118.8	59.2	4	This study
Ni-Fe/Al_2O_3	900	180.6	63.4	4	This study
Ni-Fe/Al_2O_3 dried	700	146.8	70.2	4	This study
25Fe+75Co	800	30	24	5	[20]
50Fe+50Co	800	60	44	5	[20]
75Fe+25Co	800	40	33	5	[20]

4. CONCLUSIONS

This study investigated Fe–Ni catalysts supported on γ-Al_2O_3 for methane pyrolysis, comparing as-synthesized samples with those who overcame drying pre-treatment. Surface chemistry, structural properties, and reaction outcomes were analysed using XPS, FTIR, Raman spectroscopy, XRD, and mass spectrometry.

The results indicated that catalyst drying altered surface and lattice oxygen states, as observed by XPS, which affected methane activation and the resulting hydrogen production efficiency. Structural analyses revealed variations in carbon defect density and crystallinity, with a noticeable increase in the carbon-related diffraction peaks in XRD and well-defined D and G bands in Raman spectra. The type and quality of deposited carbon were expected to influence its potential applications and value. Notably, dried catalysts exhibited a 6–8% higher hydrogen yield compared to as-synthesized samples across all tested temperatures, highlighting the importance of catalyst pre-treatment in enhancing turquoise hydrogen production efficiency.

ACKNOWLEDGEMENTS

To the M-EraNet call project INNOHYPPY, for received financial support from the Latvian Scientific Council No. ES RTD/2023/15 and the Research Council of Lithuania agreement No. S-MERANET-23-1/PFS_INNOH_23-1.

REFERENCES

1. European Commission. (2020). *Hydrogen Strategy for a Climate-Neutral Europe*, COM(2020) 301 Final. Brussels. Available at https://energy.ec.europa.eu/system/files/2020-07/hydrogen_strategy_0.pdf
2. Staffell, I., Scamman, D., Velazquez Abad, A., Balcombe, P., Dodds, O. E., Ekins, P., … & Ward, K. R. (2019). The Role of Hydrogen and Fuel Cells in the Global Energy System. *Energy & Environmental Science*, *12*, 463–491. https://doi.org/10.1039/C8EE01157E
3. Phogat, P., Chand, B., & Shreya. (2025). Hydrogen Economy: Pathways, Production Methods, and Applications for a Sustainable Energy Future. *Sustainable Materials and Technologies, 45*. https://doi.org/10.1016/j.susmat.2025.e01550
4. Abánades, H., Rubbia, C., & Salmieri, D. (2013). Thermal Cracking of Methane into Hydrogen for a CO2-Free Utilization of Natural Gas. *Int. J. of Hydrogen Energy., 38* (20), 8491–8496. https://doi.org/10.1016/j.ijhydene.2012.08.138
5. Swartbooi, A., Kapanji-Kakoma, K. K., & Musyoka, N. M. (2022). From Biogas to Hydrogen: A Techno-Economic Study on the Production of Turquoise Hydrogen and Solid Carbons. *Sustainability, 14* (17), 11050. https://doi.org/10.3390/su141711050
6. Bayat, N., Rezaei, M., & Meshkani, F. (2016). Methane Decomposition over Ni–Fe/Al2O3 Catalysts for Production of COx-Free Hydrogen and Carbon Nanofiber. *Int. J. of Hydrogen Energy, 41 (3),* 1574–1584. https://doi.org/10.1016/j.ijhydene.2015.10.053
7. Wang, P., Zhu, H., Huang, M., Wan, C., Li, D., & Jiang, L. (2022). Catalytic Methane Decomposition to Hydrogen and Carbon over Hydrotalcite-Derivative Composition-Uniform and Sintering-Resistant Ni-Fe/Al2O3 Alloy Catalysts. *Int. J. Energy Res., 46,* 16810–16822. https://doi.org/10.1002/er.8349
8. Karaismailoğlu, M., Figen, H. E., & Baykara, S. Z. (2020). Methane Decomposition over Fe-based Catalysts. *Int. J. Hydrogen Energy*, *45* (60), 34773–34782. https://doi.org/10.1016/j.ijhydene.2020.07.219
9. Khaleel, A., Adamson, A., & Pillantakath, A.-R. (2024). The Impact of Surface-Impregnated versus Support-Dispersed Fe in Fe–Ni/γ-Al_2O_3 Catalysts for Partial Oxidation of Methane: Insights into the Effect of Fe Incorporation Method on Coking and on the Reaction Mechanism. *Int. J. Hydrogen Energy, 81,* 643–653. https://doi.org/10.1016/j.ijhydene.2024.07.191
10. Esteves, L. M., Daas, A. A., Oliveira, H. A., & Passos, F. B. (2020). Effect of Catalyst Pretreatment on Ni-based Catalysts for Methane Decomposition. *Int. J. Hydrogen Energy, 45* (51), 27299–27311. https://doi.org/10.1016/j.ijhydene.2020.07.133
11. Azancot, L., Bobadilla, L. F., Santos, J. L., Cordoba, J. M., Centeno, M. A., & Odriozola, J. A. (2019). Influence of the Preparation Method in the Metal-Support Interaction and Reducibility of Ni-Mg-Al Based Catalysts for Methane Steam Reforming. *Int. J. Hydrogen Energy, 44* (36). 19827–19840. https://doi.org/10.1016/j.ijhydene.2019.05.167
12. Laybo, D., Etim, U. J., Monai, M., Bare, S. R., Zhong, Z., & Vogt, C. (2024). Metal–Support Interactions in Metal Oxide-Supported Atomic, Cluster, and Nanoparticle Catalysis. *Chem. Soc. Rev., 53,* 10450–10490. https://doi.org/10.1039/D4CS00527A

13. Ferrari, A. C., & Robertson, J. (2000). Interpretation of Raman Spectra of Disordered and Amorphous Carbon. *Phys. Rev. B*, *61*, 14095–14107. https://doi.org/10.1103/PhysRevB.61.14095
14. El-Maghraby, A., El-Deeb, H. A., & Khattab, M. A. (2015). Influence of FeNi/Al2O3 Catalyst Compositions on the Growth of Carbon Nanotubes. *Fullerenes, Nanotubes and Carbon Nanostructures 23* (1). https://doi.org/10.1080/1536383X.2012.702159
15. Shekhar, S., Tripathi, K., Karton, A., Roy, S., Joshi, R., & Pant, K. K. (2025). Influence of Ni on Carbon Nanotube Production with Fe-based Catalysts. *Chem. Commun., 61,* 2063–2066. https://doi.org/10.1039/D4CC05698A
16. Sun, E., Zhai, S., Kim, D., Gigantino, M., Haribal, V., Dewey, O. S., … & Majumdar, A. (2023). A Semi-Continuous Process for Co-production of CO2-Free Hydrogen and Carbon Nanotubes via Methane Pyrolysis. *Cell Reports Physical Science*, *4* (4), 101338. https://doi.org/10.1016/j.xcrp.2023.101338
17. Wang, I. W., Kutteri, D. A., Gao, B., Tian, H., & Hu, J. (2019). Methane Pyrolysis for Carbon Nanotubes and CO_x -Free H_2 over Transition-Metal Catalysts. *Energy and Fuels*, *33* (1), 197–205. https://doi.org/10.1021/acs.energyfuels.8b03502
18. Wang, D., Zhang, J., Sun, J., Gao, W., & Cui, Y. (2019). Effect of Metal Additives on the Catalytic Performance of Ni/Al_2O_3 Catalyst in Thermocatalytic Decomposition of Methane. *Int. J. of Hydrogen Energy*, *44* (14), 7205–7215. https://doi.org/10.1016/j.ijhydene.2019.01.272
19. Zhang, W., Gao, L., Zhang, M., Cui, J., Li, Y., Gao, L., & Zhang, S. (2014). Methane Catalytic Cracking to Make Hydrogen and Graphitic Nano Carbons (Nanotubes, Microfibers, Microballs, Onions) with Zero Emission. *Synthesis and Reactivity in Inorganic, Metal-Organic and Nano-Metal Chemistry, 44* (8), 1166–1174. https://doi.org/10.1080/15533174.2013.797452
20. Al-Fatesh, A.S., Abdelkader, A., Osman, A. I., Lanre, M. S., Fakeeha, A. H., Alhoshan, M., … & Rooney, D. W. (2023). Non-supported Bimetallic Catalysts of Fe and Co for Methane Decomposition into H_2 and a Mixture of Graphene Nanosheets and Carbon Nanotubes. *Int. J. of Hydrogen Energy, 48* (68), 26506–26517. https://doi.org/10.1016/j.ijhydene.2022.10.223